

AUTOMATION AND CONTROL LABORATORY

ROTATING MASSES EXPERIMENT

MATTEO ESPOSITO - matteo2.esposito@mail.polimi.it - 10538105

GIUSEPPE LONGO - giuseppe4.longo@mail.polimi.it - 10752114

GIOVANNI PORCELLATO - giovanni.porcellato@mail.polimi.it - 10745779

FRANCESCO SACCHI - francesco6.sacchi@mail.polimi.it - 10799907

Academic Year - 2021-2022

Contents

1 One-mass configuration	3
1.1 1-DOF Dynamic and State-Space Model	4
1.2 1-DOF Model Identification and Validation	5
1.3 Open-Loop Analysis	8
1.3.1 Position Output	8
1.3.2 Speed Output	9
1.4 Closed-Loop Control	10
1.4.1 PID Attempt	10
1.4.2 Loop Shaping Compensators	12
2 Two-masses configuration	19
2.1 2-DOF Dynamic and State-Space Model	20
2.2 2-DOF Model Identification and Validation	21
2.3 Open-Loop Analysis	23
2.3.1 Position output	23
2.3.2 Speed output	24
2.4 Closed-Loop Analysis	25
2.4.1 Position Control	30
2.4.2 Speed Control	35
3 Conclusions	38

1 One-mass configuration

The Quanser Torsion module is a rotary torsional system that consists of an instrumented bearing block, which is mounted in a cubic solid aluminum frame. A shaft is free to spin inside the bearing block. The shaft rotation is measured using an encoder. The shaft can be outfitted with either a pulley or a flexible coupling. The system is designed to couple with a Quanser rotary servo, in our case SRV02. As illustrated in Figure 1.1, below, the assembly made of one rotary Torsion module coupled to a SRV02 servo plant constitutes a one-Degree-Of-Freedom (1-DOF) torsional system.

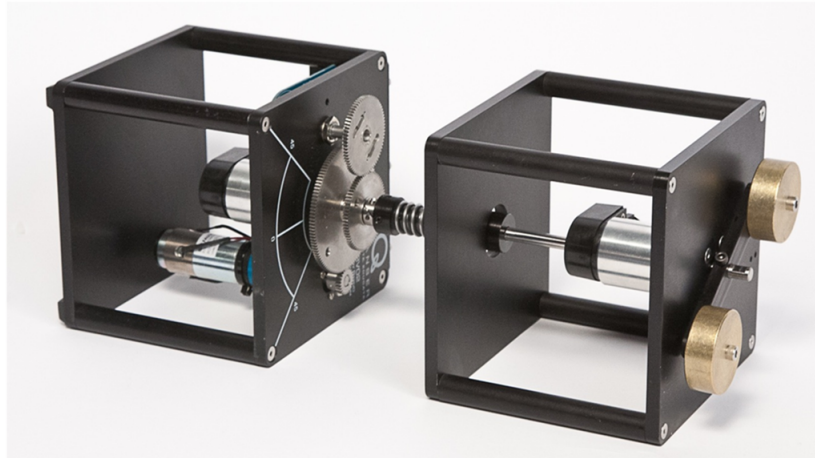


Figure 1.1: 1-DOF real setup

The SRV02 unit lies on its side so that its DC motor and output shaft are horizontal and able to rotate a flexible coupling attached to a rotational load. The torsional load consists of two inertial disc masses, which can be located at different anchor points along their support bar. Several torsion modules can be coupled in cascade to allow for multidimensional control problems (up to seven).

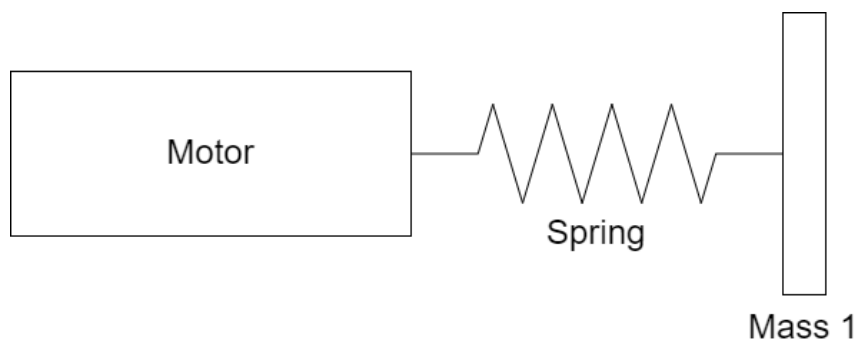


Figure 1.2: 1-DOF system schematic representation

1.1 1-DOF Dynamic and State-Space Model

Starting from mechanical considerations, D'Alembert equations can be written in order to describe the dynamics of the systems.

The first equation is related to the motor side:

$$J_1 \ddot{\theta}_1 + B_1 \dot{\theta}_1 + k_s (\theta_1 - \theta_2) = \tau_1 \quad (1.1)$$

The second equation is related to the load side:

$$J_2 \ddot{\theta}_2 + B_2 \dot{\theta}_2 + k_s (\theta_2 - \theta_1) = 0 \quad (1.2)$$

Where:

J is the moment of inertia

B is the coefficient of viscous friction

k_s is the spring stiffness

τ_1 is the torque applied by the motor

Finally, from the electromechanical relations, the following expression of the motor couple is obtained:

$$\tau_1 = \left(\frac{\eta_g k_g \eta_m k_t}{R_m} \right) V_{DC} - \left(\frac{\eta_g k_g \eta_m k_t}{R_m} \right) \dot{\theta}_1 \quad (1.3)$$

State-space model The state-space model is defined as follows:

$$\begin{bmatrix} \dot{q} \\ y \end{bmatrix} = \begin{bmatrix} Aq + Bu \\ Cq \end{bmatrix} \quad (1.4)$$

The state variables are:

$$\begin{aligned} q_1 &= \theta_1 \\ q_2 &= \dot{q}_1 = \dot{\theta}_1 \\ q_3 &= \theta_2 \\ q_4 &= \dot{q}_3 = \dot{\theta}_2 \end{aligned} \quad (1.5)$$

The state-space matrix can be summarized as:

$$\begin{bmatrix} \dot{q}_1 \\ \dot{q}_2 \\ \dot{q}_3 \\ \dot{q}_4 \end{bmatrix} = \begin{bmatrix} 0 & 1 & 0 & 0 \\ a_{21} & a_{22} & a_{23} & 0 \\ 0 & 0 & 0 & 1 \\ a_{41} & 0 & a_{43} & a_{44} \end{bmatrix} \begin{bmatrix} q_1 \\ q_2 \\ q_3 \\ q_4 \end{bmatrix} \begin{bmatrix} 0 \\ b_2 \\ 0 \\ 0 \end{bmatrix} [V_{DC}] \quad (1.6)$$

$$a_{21} = -\frac{k_s}{J_1} \quad a_{22} = -\left(\frac{B_1}{J_1} + \frac{\eta_g k_g^2 \eta_m k_t k_m}{R_m J_1} \right) \quad a_{23} = \frac{k_s}{J_1} \quad a_{41} = \frac{k_s}{J_2}$$

$$a_{43} = -\frac{k_s}{J_2} \quad a_{44} = -\frac{B_2}{J_2} \quad b_2 = \frac{\eta_g k_g \eta_m k_t}{R_m J_1}$$

1.2 1-DOF Model Identification and Validation

After developing the mathematical model, the gray box approach was the most appropriate way to estimate the parameters of the system.

Initially, through the input/output approach, several experiments were performed on both systems, the real and the simulated one, with input signals at different frequencies and amplitudes, hence the output of the system was collected.

Afterwards, the difference between simulated output and the measured one was defined, with the aim of minimizing it.

The idea was to start from the nominal parameters and then use an iterative minimization to fit them to the real system. This optimization was performed using the MATLAB function `fmincon`. The cost function was defined as the difference between the measured outputs and the simulated ones with the same inputs.

The identification analysis ended up in 11 uncertain physical parameters of the system to be tuned. Another solution was to reduce the number of parameters defining some of them as ratios of the initial ones. Some simulations were performed, but results were not good, because the interdependence between some parameters is too strong and it is difficult to choose the variables to combine. Moreover, the minimization problem with 11 variables is solvable in allowable computational times, so it is pointless to try to reduce the number of variables adding constraints due to interdependences.

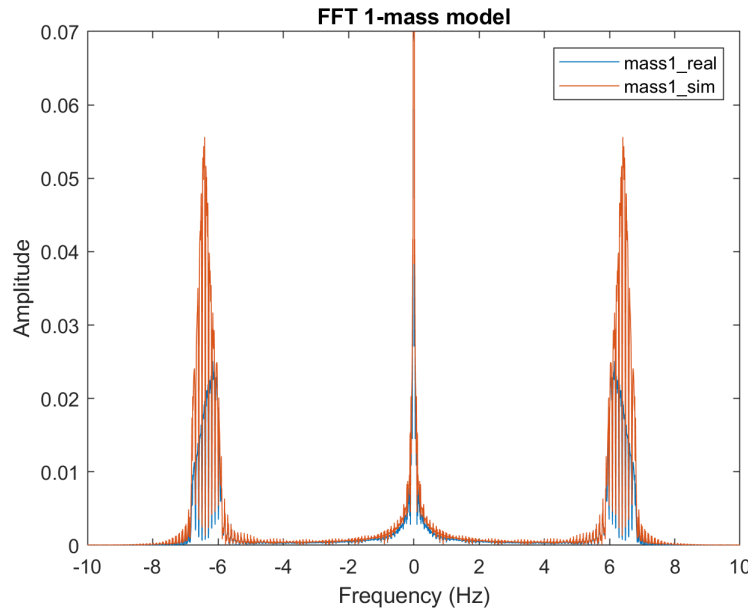


Figure 1.3: 1-mass FFT comparison between real and simulated configurations

The FFT in Figure 1.3 is a graphical validation of the mathematical model. The simulated configuration has a resonant peak that corresponds to the one of the real system, despite it is more prominent due to the fact that frictions were neglected.

Models comparison The following figures report some outcomes of the experiments that were performed for the identification, comparing the output of the real system with the outputs of the simulated model, both with the nominal and with the optimized parameters. In correlation with the developed dynamical model, θ_1 is the motor angle, while θ_2 is the mass angle.

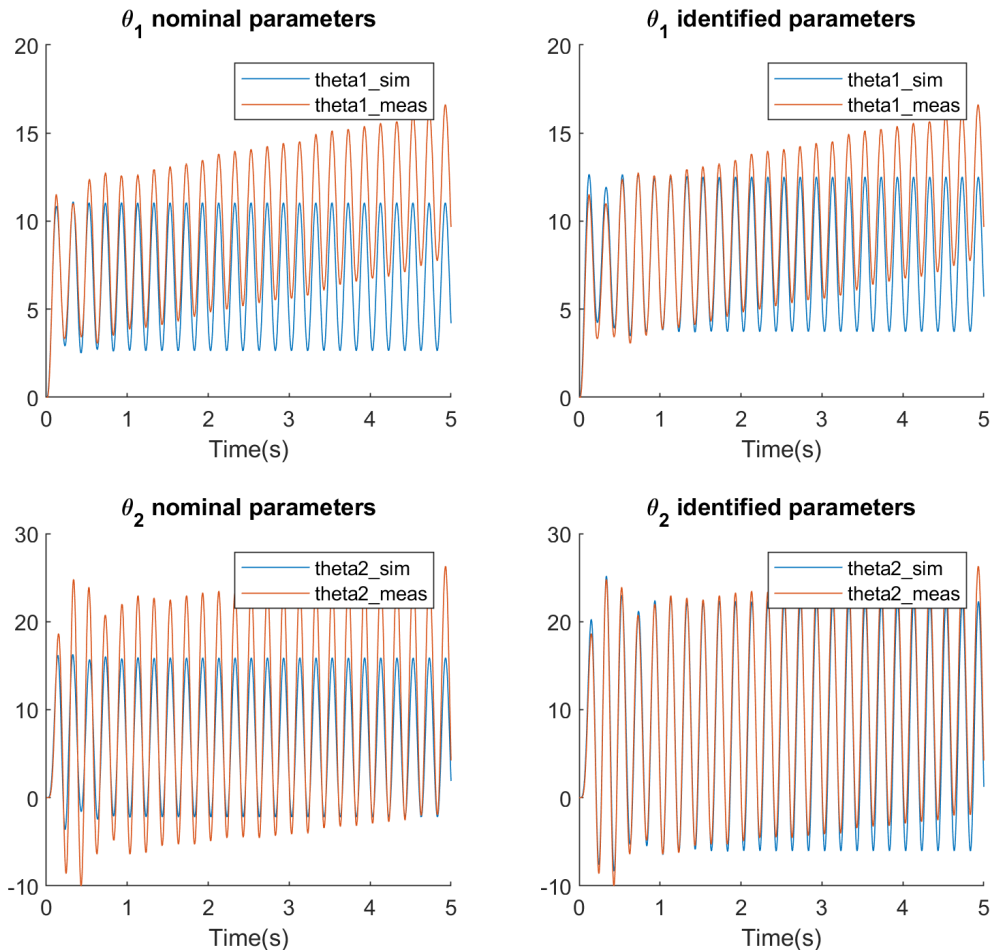


Figure 1.4: Simulation with amplitude of 2.5 and frequency 5 Hz

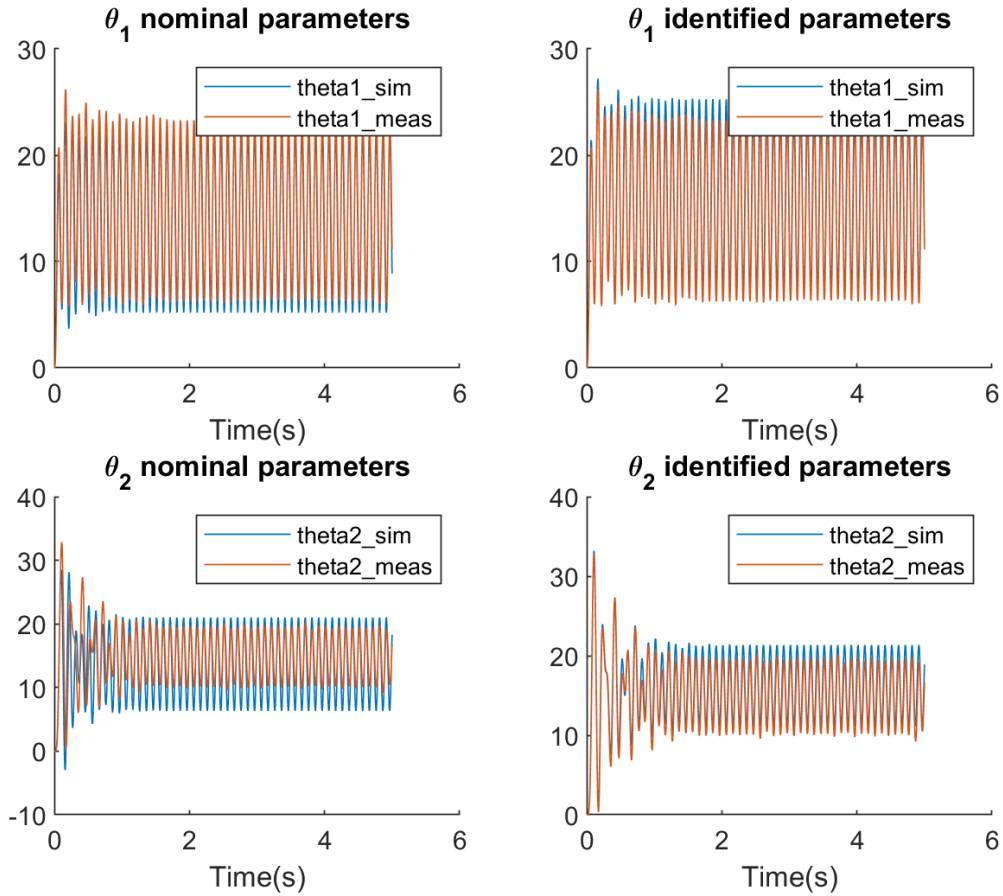


Figure 1.5: Simulation with amplitude of 10 and frequency 10 Hz

From these experiments it is possible to notice the different behaviours between the simulated system with nominal parameters (on the left) and the one with identified parameters (on the right).

This mismatch comes from the approximations used by the theoretical model, as already discussed. With the identified parameters, these approximations could be compensated and the simulated model becomes closer to the real one.

1.3 Open-Loop Analysis

Once the model of the system was defined, the transfer functions related to velocity and position were extracted and their Bode diagrams were analyzed to study the stability properties. In the Bode diagrams of both the transfer functions, there is a marked peak of resonance caused by the two complex conjugate poles at frequency of about 40 rad/s. This peak brings a huge instability and related control problems.

1.3.1 Position Output

The transfer function from input to the angular position of the mass is the following (in zero-pole notation form):

$$\frac{92745}{s(s + 31.91)(s^2 + 5.322s + 1632)} \quad (1.7)$$

The Bode Diagram below shows a positive phase margin and a finite gain margin, so the system is closed-loop stable. From a performance point of view, the cut-off frequency is too small, leading to a slow response and a short bandwidth not good for high frequency input signals.

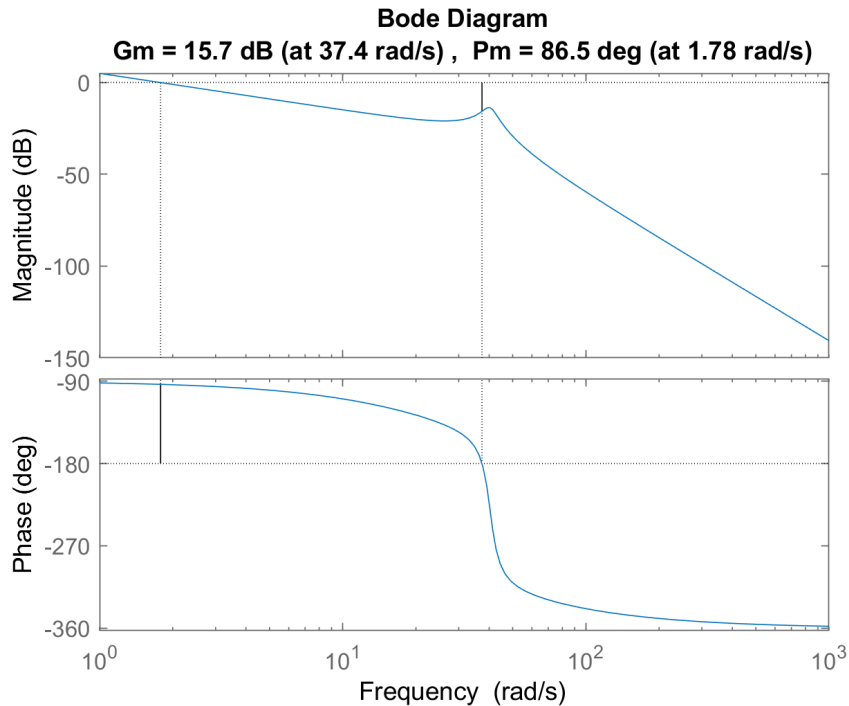


Figure 1.6: 1-DOF position Bode diagram

1.3.2 Speed Output

The transfer function from input to the angular speed of the mass is the following (in zero-pole notation form):

$$\frac{92745}{(s + 31.91)(s^2 + 5.322s + 1632)} \quad (1.8)$$

The zero due to the derivative action leads to the cancellation of the pole in zero. Accordingly, the corresponding Bode diagram is equivalent to the position one, except for the gain, which is constant at frequencies lower than the resonance one, and for the initial phase, which starts from 0 degrees. This takes to a totally unstable closed-loop system; moreover the resonant peak remains totally uncut.

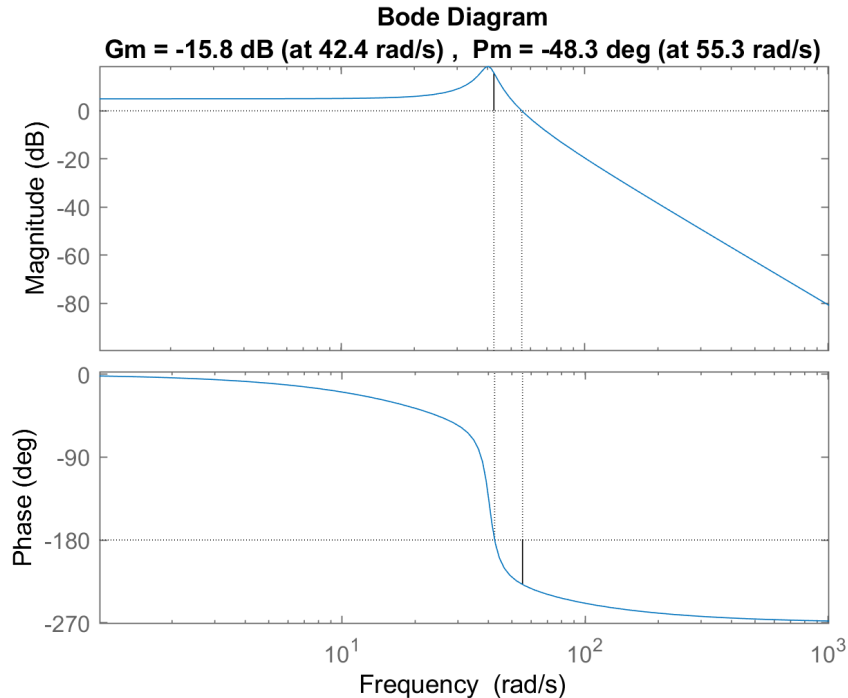


Figure 1.7: 1-DOF speed Bode diagram

1.4 Closed-Loop Control

1.4.1 PID Attempt

The first attempt of control consisted in a PID regulator. The performance obtained with this control was not acceptable, so other techniques were developed, more specific for the system, leading to better settling and rise times.

For these reasons, this first solution will be discussed briefly.

P for position In order to control the position of the mass, the P regulator has the following control law:

$$V_m(t) = k_p(\theta_{ref}(t) - \theta_m(t)) \quad (1.9)$$

where k_p is the proportional gain, θ_{ref} is the reference load angle and θ_m is the measured load angle. The resulting V_m is the motor input voltage. The tuning of k_p was performed in a *trial and error* way starting from values obtained by the Ziegler-Nichols closed-loop method.

In this approach all the parameters are function of K_{cr} and T_{cr} , i.e. critical gain and critical period. The idea is to gradually increase the value of the closed-loop gain until you get an unstable situation: this will be the K_{cr} gain, while the resulting instability oscillations will determine the T_{cr} period.

In our case $K_{cr} = 5$ and $T_{cr} = 4.7$ s.

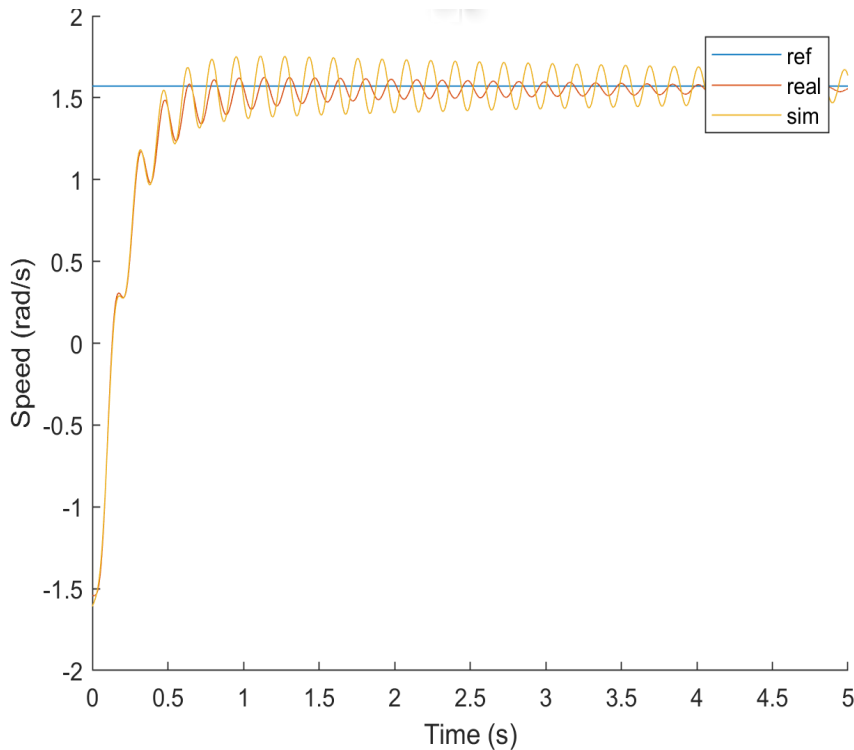


Figure 1.8: Position output step response with P controller

	Rise Time	Settling time 3%
Real system	0.37 s	1.56 s
Simulated system	0.364 s	4.98 s

The step response above shows an interesting result about the friction action, that leads to less oscillating behaviour for the real system and to better settling time, compared to the simulated one. Anyway, the result is not acceptable.

PI for speed Here, the adopted tuning idea is the same as before (closed-loop Ziegler-Nichols). Nonetheless, in this case the absence of a pole in zero (due to the derivative action) leads to a steady-state error. To remove it, an integral action is needed and the controller becomes a PI.

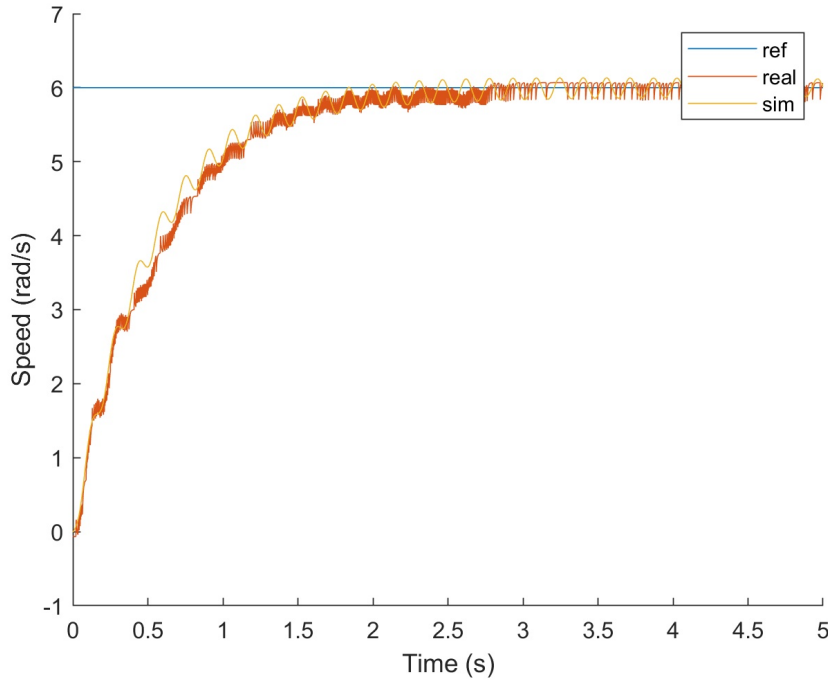


Figure 1.9: Speed output step response with PI controller

	Rise Time	Settling time 3%
Real system	1.11 s	2.90 s
Simulated system	0.98 s	2.70 s

In this case, the performance indices of the actual response and of the simulated one are comparable. The oscillating behaviour remains in common with what seen on position control case. Even in this case, the settling time is too long and not acceptable.

1.4.2 Loop Shaping Compensators

The final decision for the control fell on a custom regulator, designed in a similar way to the loop shaping method, both for reference tracking and for disturbance rejection, slightly modifying the type of controller depending on the case.

The controller design must include a direct action against the severe resonant peak, in order to reduce its effect. Since the resonance derives from the action of two complex-conjugate poles with a low damping factor, the idea was to place an anti-resonance (i.e., two complex and conjugate zeros) at the corresponding frequency, in order to attenuate it. Then, gains and real poles/zeros were added in order to tune the overall performance of the system. Poles were also needed to have at least as many poles as zeros, so that the controllers are feasible. The compensation cannot be exact, because of the model approximations, so the peak remains visible, especially in the phase plot. This leads to an oscillating behaviour before the response settles.

Speed controller The speed controller develops the idea expressed above:

$$5 \frac{s^2/1616 + 5/1616 s + 1}{s(s/90 + 1)^2} \quad (1.10)$$

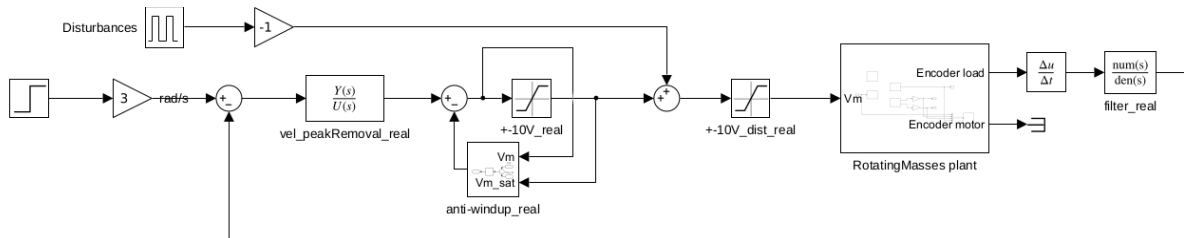


Figure 1.10: Loop Shaping speed control scheme

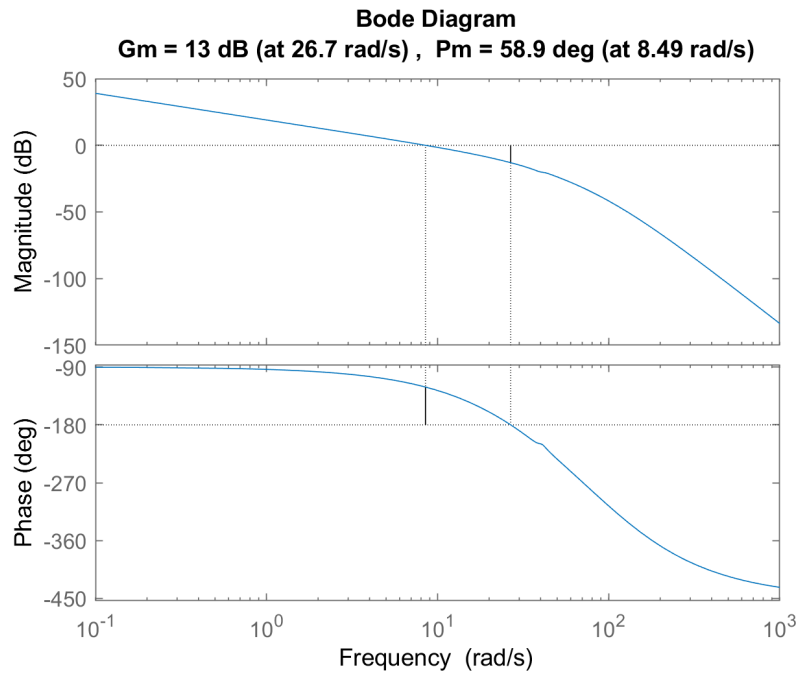


Figure 1.11: Controlled system Bode plot

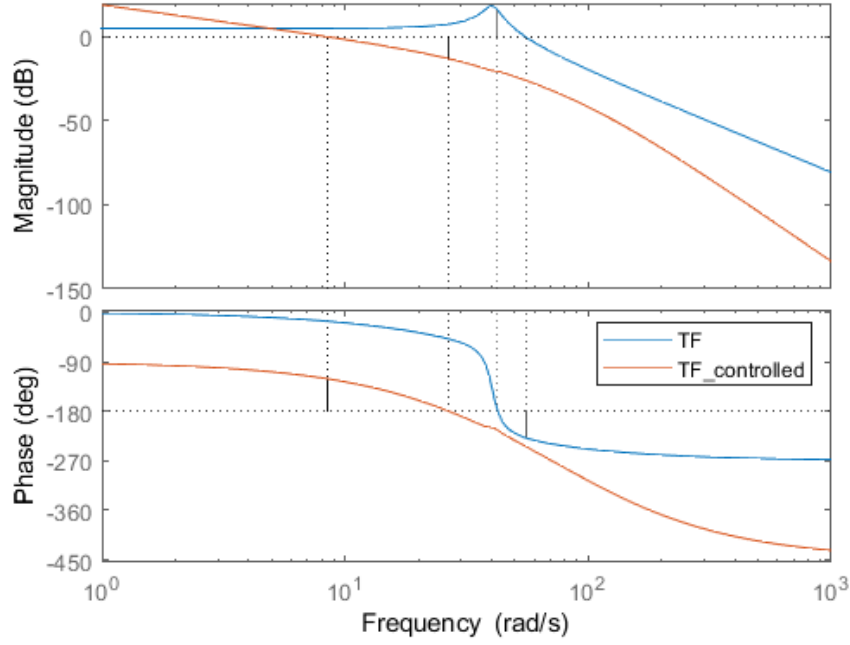


Figure 1.12: Controlled system Bode plot comparison

In the Figure 1.11, the Bode diagram of the closed-loop transfer function of the speed is plotted.

The diagram shows the gain and phase margins of the controlled speed. The parameters are chosen to maximize the performance, i.e. to have the best margins and cutoff frequency. With this choice, the behaviour of the system is the following:

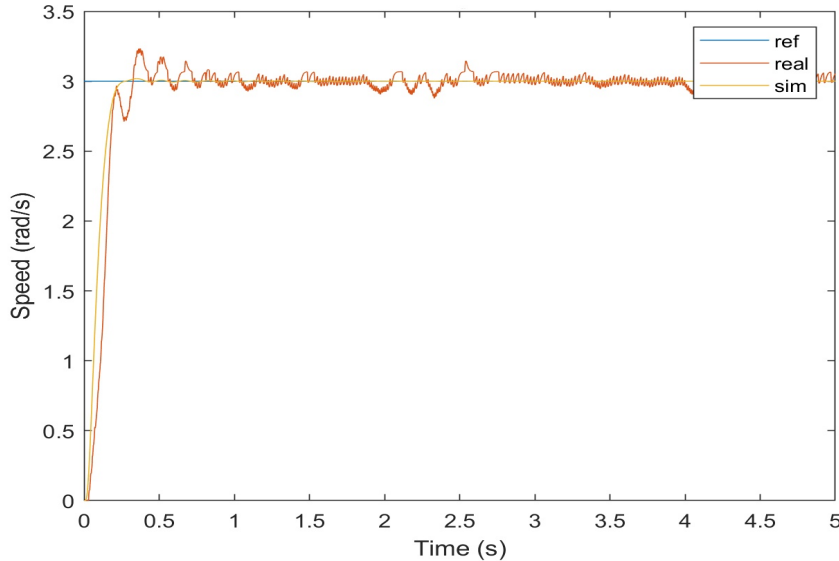


Figure 1.13: Speed output step response with Loop Shaping controller

Where the settling time is very short and the oscillations are low. The Figure 1.12 compares the initial transfer function Bode diagram with the controlled transfer function one. Theoretically, the peak is completely removed. However, the oscillations in the response have frequency equal to the resonance one, showing that the peak is not perfectly cancelled and the system is still slightly subject to it.

The input voltage has a behaviour that is similar to the simulated one, except that it is a bit larger. Probably, this is due to some sliding frictions that were not modelled.

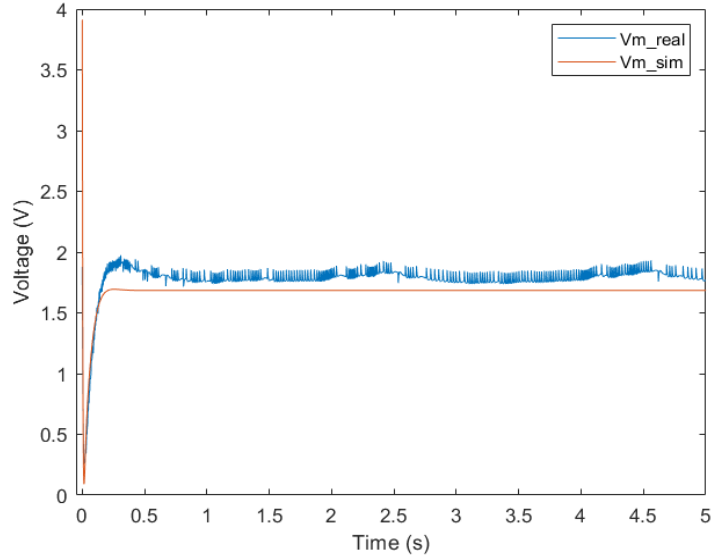


Figure 1.14: V_m input speed step response with Loop Shaping controller

	Rise Time	Settling time 3%
Real system	0.130 s	0.696 s
Simulated system	0.128 s	0.204 s

For the disturbance attenuation, the controller defined above was modified. A zero was added in correspondence of the resonance frequency, in order to increase the phase margin, without moving the crossover frequency. In this way, it was possible to obtain a similar performance in terms of settling time, with greater robustness.

Below, the transfer function is reported and its Bode diagram is plotted, as well as the response of the system to disturbances and the input voltage.

$$6 \frac{(s^2/1616 + 5/1616 s + 1)(s/41 + 1)}{s(s/120 + 1)^2} \quad (1.11)$$

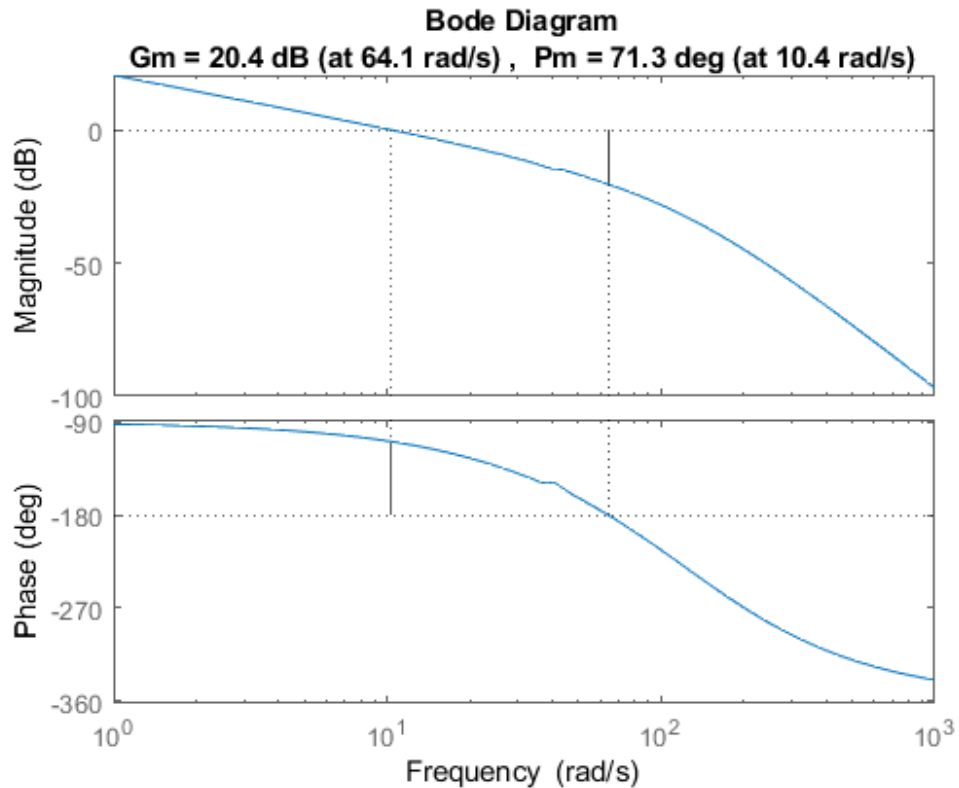


Figure 1.15: Bode diagram of system controlled for disturbance rejection

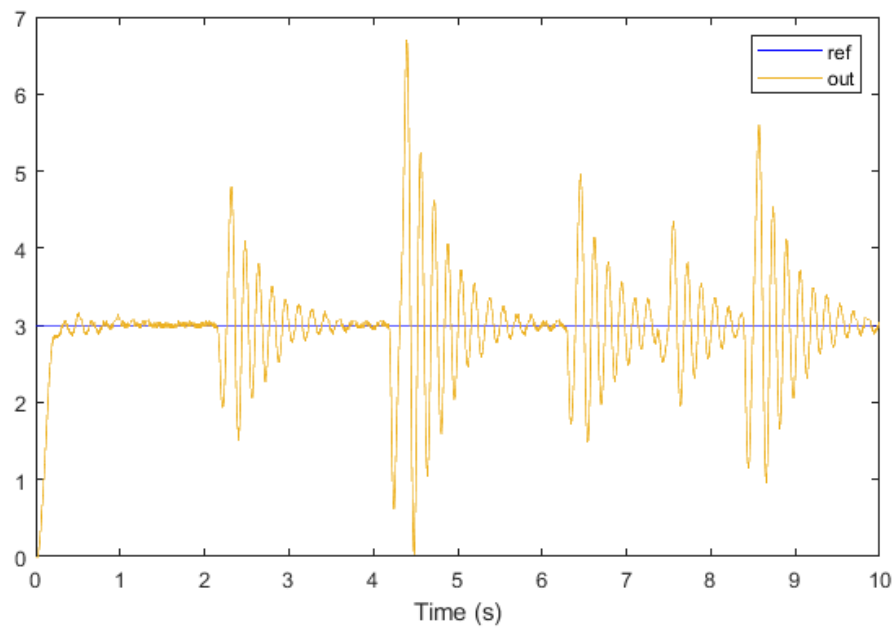


Figure 1.16: Velocity control output of the disturbed system

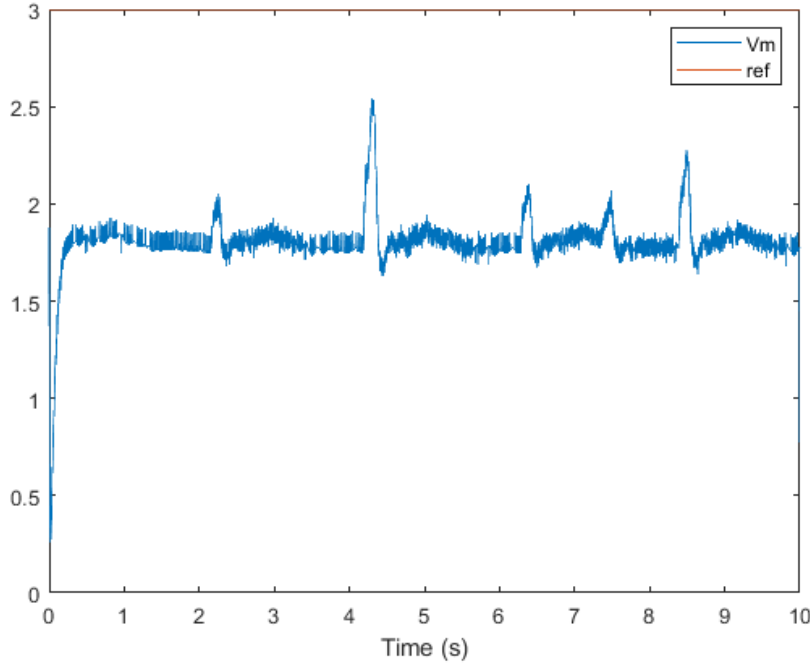


Figure 1.17: Input voltage of the disturbed system

The plot of the input voltage shows that the controller requires a higher voltage when the mass is perturbed and its speed is modified, in order to recover it.

Position control Initially, the same approach as above was used. Here, the open-loop transfer function already had a pole in zero, that looked enough to avoid steady-state error. The resulting transfer function cancelled the peak and its Bode diagram was:

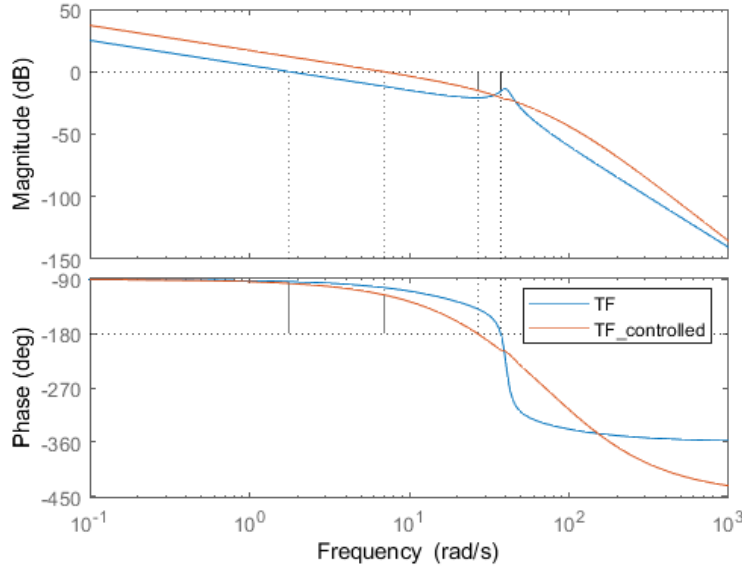


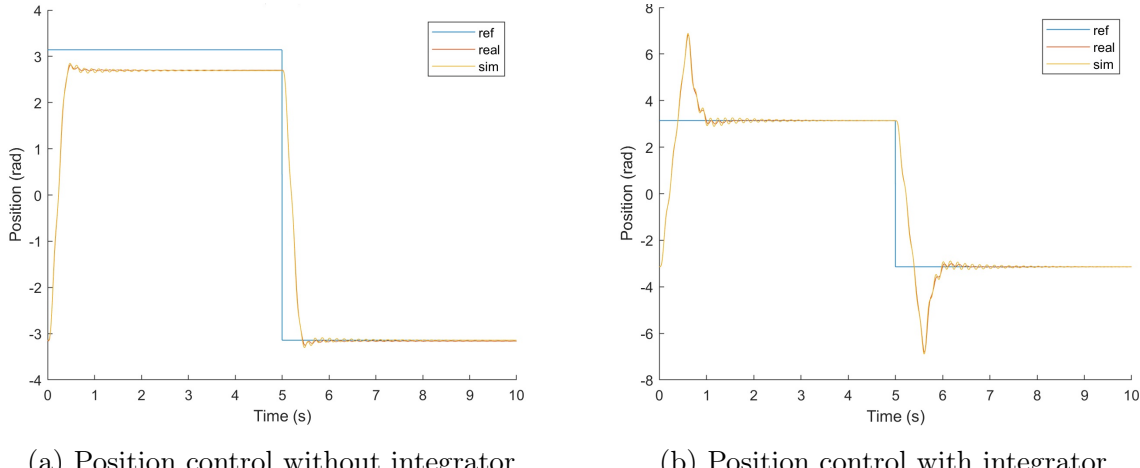
Figure 1.18: Bode diagram comparison

The Figure 1.17 shows how the resonance peak is removed.

However, with this controller the steady-state error does not tend to 0 (Figure a).

Then, an integrator was added, but also other poles and zeros had to be added to ensure

stability, leading to a performance that is not acceptable (particularly referring to the overshoot and the settling time, Figure b).



The proposed solution is a cascade control. The outer loop performs position control, with a simple P regulator. The inner loop performs speed control, applying the control strategy that was introduced above (in particular, the controller used for disturbance rejection). If the stabilized inner loop is sufficiently fast, the outer loop sees it as a unitary transfer function, so a proportional controller is enough to guarantee stability and its value can be tuned to improve the performance (4 appeared to be the best one).

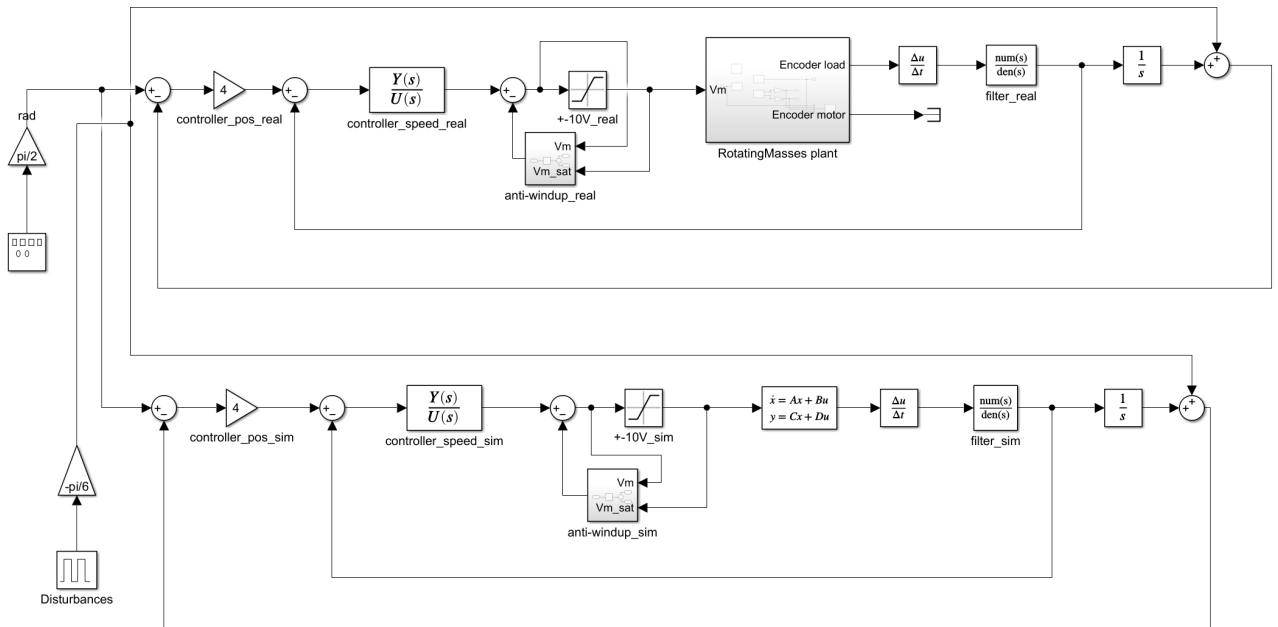


Figure 1.20: Loop Shaping position cascade control

In this way, the system provides optimal results in both performance and noise rejection, as it is shown in figure 1.21 and 1.22.

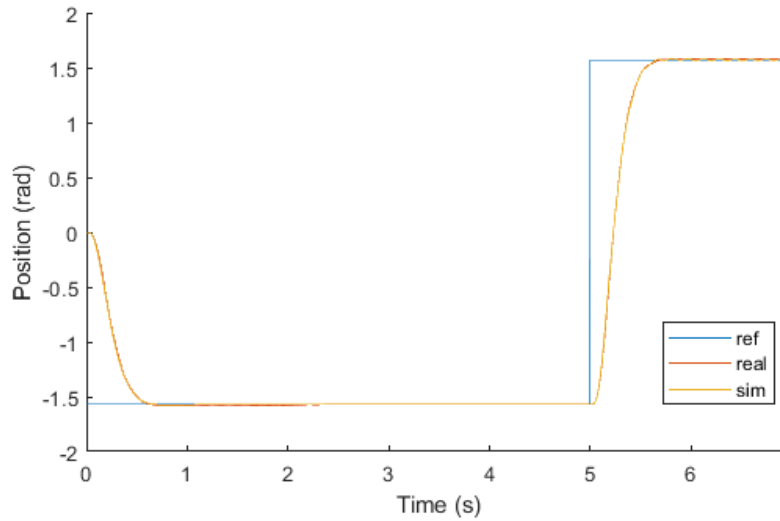


Figure 1.21: Position reference tracking with cascade control

	Rise Time	Settling time 3%
Real system	0.324 s	0.530 s
Simulated system	0.324 s	0.532 s

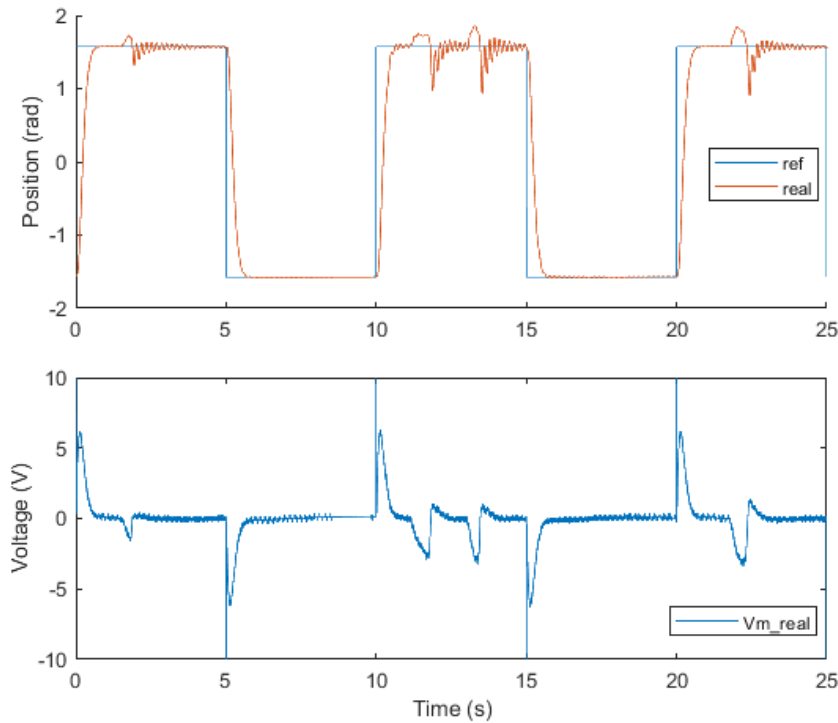


Figure 1.22: Disturbance rejection of system with cascade control

Even the input voltage is plotted, showing that the controller requires higher voltages when a disturbance is applied.

2 Two-masses configuration

The Two-Degree-Of-Freedom (2-DOF) torsional configuration is shown in Figure 1.2, below, where two rotary Torsion modules are mounted in series with an SRV02 servo plant. Similarly to the 1-DOF Torsion system, the SRV02 lies on its side such that its DC motor and output shaft are horizontal and able to rotate the two cascaded flexible couplings, each attached to a rotational load. Each torsional load consists of two inertial disc masses, which can be located at different anchor points along their support bar.

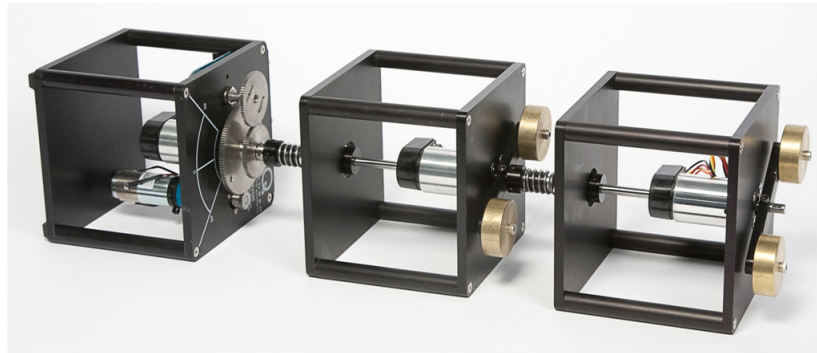


Figure 2.1: 2-DOF real setup

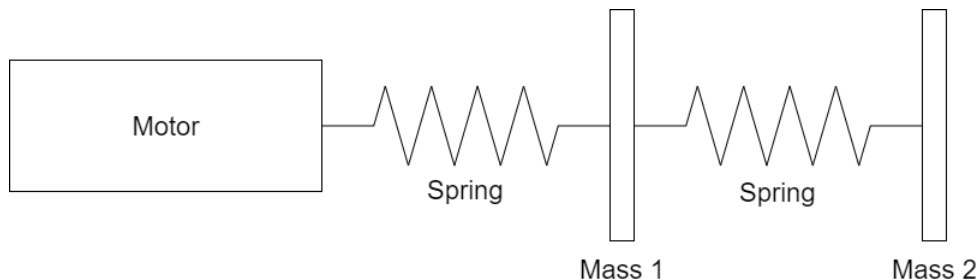


Figure 2.2: 2-DOF system schematic representation

2.1 2-DOF Dynamic and State-Space Model

Similarly to the one mass case, the dynamic model for the complete system was derived . The first equation comes straightforward from the previous case:

$$J_1 \ddot{\theta}_1 + B_1 \dot{\theta}_1 + k_s (\theta_1 - \theta_2) = \tau_1 \quad (2.1)$$

The second equation is modified due to the influence of the third mass:

$$J_2 \ddot{\theta}_2 + B_2 \dot{\theta}_2 + k_s (\theta_2 - \theta_1) + k_s (\theta_2 - \theta_3) = 0 \quad (2.2)$$

The third mass is considered by adding another equation

$$J_3 \ddot{\theta}_3 + B_3 \dot{\theta}_3 + k_s (\theta_3 - \theta_2) = 0 \quad (2.3)$$

State Space Model Similarly to the one mass case, the state space model was developed:

$$\begin{bmatrix} \dot{q} \\ q \end{bmatrix} = \begin{bmatrix} Aq + Bu \\ Cq \end{bmatrix} \quad (2.4)$$

where input u is defined as the input voltage.

$$\begin{bmatrix} q \\ \dot{q} \end{bmatrix} = \begin{bmatrix} q_1 & q_2 & q_3 & q_4 & q_5 & q_6 \\ \dot{q}_1 & \dot{q}_2 & \dot{q}_3 & \dot{q}_4 & \dot{q}_5 & \dot{q}_6 \end{bmatrix} \quad (2.5)$$

The system state variables are:

$$\begin{aligned} q_1 &= \theta_1 \\ q_2 &= \dot{\theta}_1 = \dot{q}_1 \\ q_3 &= \theta_2 \\ q_4 &= \dot{\theta}_2 = \dot{q}_3 \\ q_5 &= \theta_3 \\ q_6 &= \dot{\theta}_3 = \dot{q}_5 \end{aligned} \quad (2.6)$$

$$\begin{bmatrix} \dot{q}_1 \\ \dot{q}_2 \\ \dot{q}_3 \\ \dot{q}_4 \\ \dot{q}_5 \\ \dot{q}_6 \end{bmatrix} = \begin{bmatrix} 0 & 1 & 0 & 0 & 0 & 0 \\ a_{21} & a_{22} & a_{23} & 0 & 0 & 0 \\ 0 & 0 & 0 & 1 & 0 & 0 \\ a_{41} & 0 & a_{43} & a_{44} & a_{45} & 0 \\ 0 & 0 & 0 & 0 & 0 & 1 \\ 0 & 0 & a_{63} & 0 & a_{65} & a_{66} \end{bmatrix} \begin{bmatrix} q_1 \\ q_2 \\ q_3 \\ q_4 \\ q_5 \\ q_6 \end{bmatrix} \begin{bmatrix} 0 \\ b_2 \\ 0 \\ 0 \\ 0 \\ 0 \end{bmatrix} [V_{DC}] \quad (2.7)$$

$$a_{21} = -\frac{k_s}{J_1} \quad a_{22} = -\left(\frac{B_1}{J_1} + \frac{\eta_g k_g^2 \eta_m k_t k_m}{R_m J_1}\right) \quad a_{23} = \frac{k_s}{J_1} \quad a_{41} = \frac{k_s}{J_2} \quad a_{43} = -2 \frac{k_s}{J_2}$$

$$a_{44} = -\frac{B_2}{J_2} \quad a_{45} = \frac{k_s}{J_2} \quad a_{63} = \frac{k_s}{J_3} \quad a_{65} = -\frac{k_s}{J_3} \quad a_{66} = -\frac{B_3}{J_3} \quad b_2 = \frac{\eta_g k_g \eta_m k_t}{R_m J_1}$$

2.2 2-DOF Model Identification and Validation

The optimization problem introduced for the single mass system was applied also to this case. The outputs measured applying sinusoidal inputs were compared to the ones obtained by the simulations with the same inputs. Minimizing the difference between the two outputs, the parameters of the two masses system were defined.

In this way, the frequency response of the simulated model is similar to the one of the physical system:

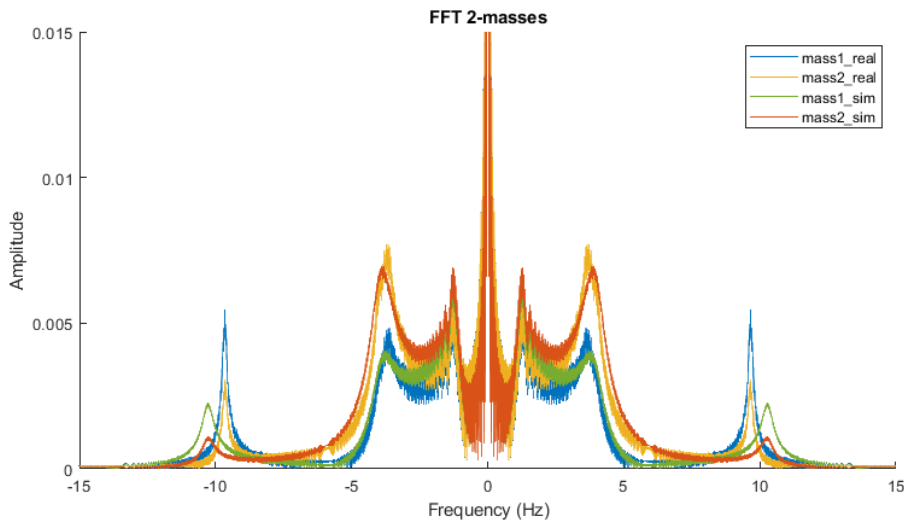


Figure 2.3: 2-DOF FFT comparison

This diagram shows also that the system has two resonances (3.6 Hz and 9.6 Hz), unlike the previous case.

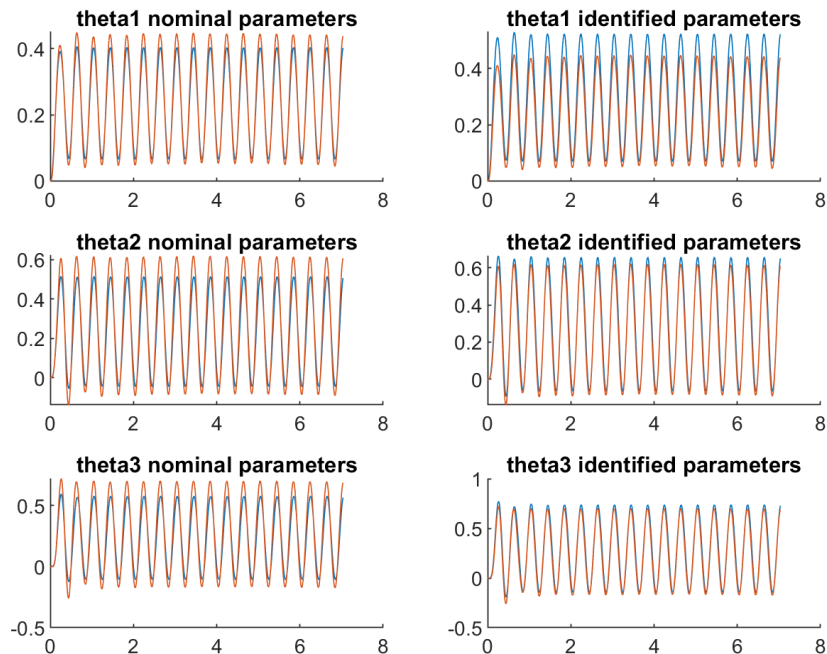


Figure 2.4: Actual and simulated outputs, input frequency: 2.5 Hz

Also the simulated outputs are closer to the actual outputs than the ones obtained with the nominal parameters, as shown in the Figures 2.4 and 2.5. The red curves are the actual outputs, whereas the blue lines show the simulated ones using the nominal parameters (left) or the optimized ones (right).

θ_1 is the motor angular position; θ_2 is the first mass angular position; θ_3 is the second mass angular position.

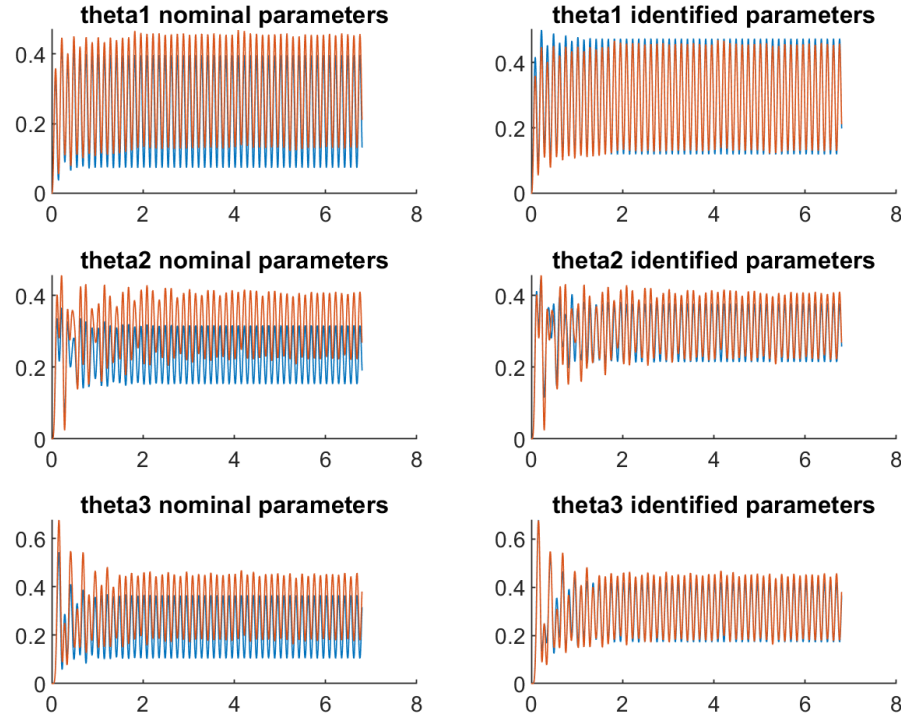


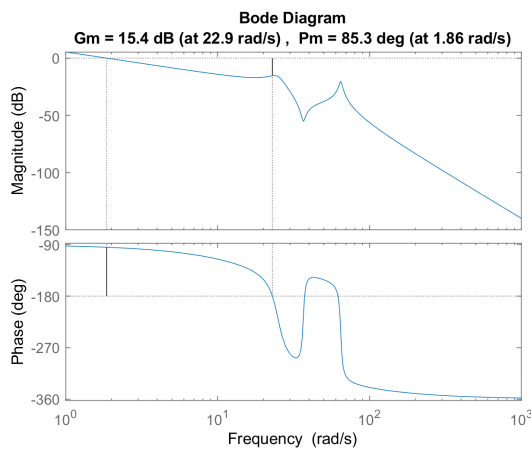
Figure 2.5: Actual and simulated outputs, input frequency: 5 Hz

2.3 Open-Loop Analysis

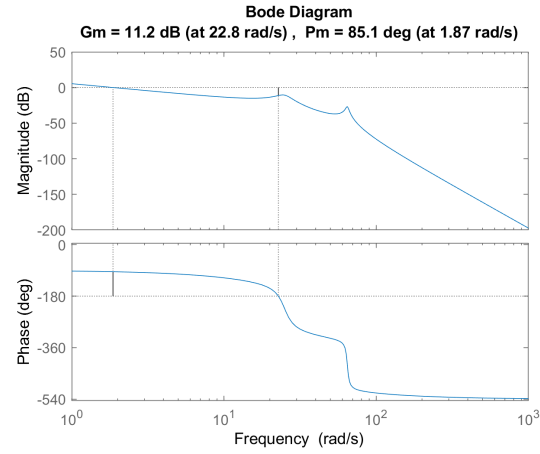
The transfer functions, both considering θ_2 and θ_3 as outputs, were computed by the mathematical model and their Bode diagrams were plotted. Besides, the open-loop system was tested both for the position and for the speed.

The transfer functions highlight the two resonances, already shown in the previous section. The control techniques for MIMO systems are different from the most common ones for SISO systems. So, the issue relating to the high resonances is solved implicitly by the designed controllers, unlike the SISO system, where the peak was explicitly removed by applying an anti-resonance.

2.3.1 Position output



(a) Bode diagram, output: θ_2



(b) Bode diagram, output: θ_3

The position open-loop was tested applying a constant input voltage, i.e. a constant speed (quite large: 8 rad/s). The input was applied for an interval of time that could be easily computed once the speed was known, allowing the angle to reach the value of $\pi/2$. The result was that both the angles increased quickly, but large, uncontrollable oscillations arose. For this reason, the settling time is very long.

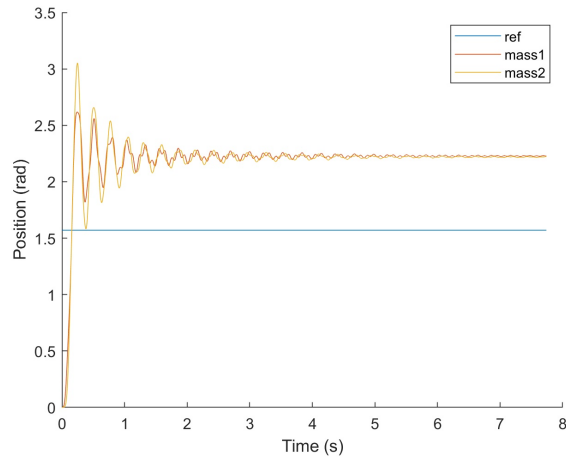
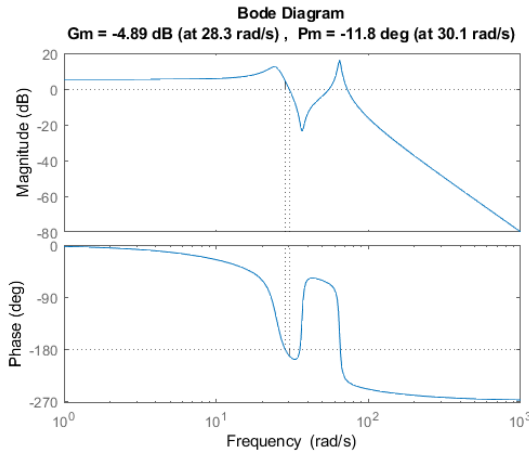
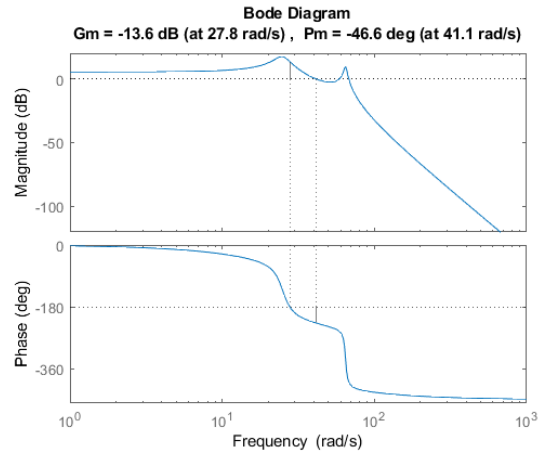


Figure 2.7: Position open-loop

2.3.2 Speed output

(a) Bode diagram, output: $\dot{\theta}_2$ (b) Bode diagram, output: $\dot{\theta}_3$

The speed open-loop was tested applying a constant input voltage giving a speed of 3 rad/s. As in the previous case, the value of the output speed increased quickly, but large oscillations were generated, extending much the settling time.

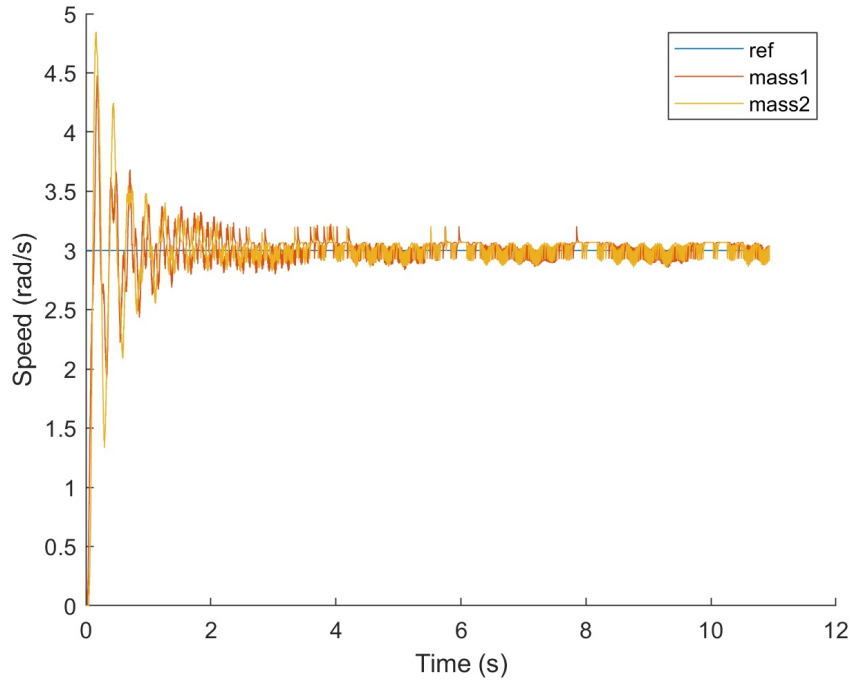


Figure 2.9: Speed open-loop

2.4 Closed-Loop Analysis

As the second mass is added, the system becomes single-input/multiple-output (SIMO). The most common control techniques for these systems require to know the whole state, so that full-state feedback can be performed. Through an observer, the non measurable states were estimated, so that the estimation could be used in the feedback.

State Observer The state observer was designed to estimate the states of the system, exploiting the input and output measurements.

$$\dot{\hat{x}}(t) = A\hat{x}(t) + Bu(t) + L[y(t) - C\hat{x}(t) - Du(t)] \quad (2.8)$$

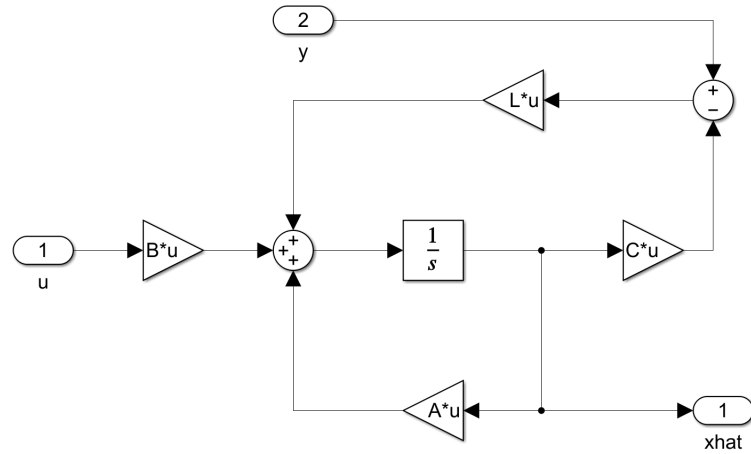


Figure 2.10: State observer model block structure

The design of the observer consists in the choice of the gain matrix L . To do it, two techniques are used, that will be shown later.

For each observer, the matrix L was then tuned by running the system in open-loop and comparing the measured quantities with the estimated ones.

Pole Placement The first approach is the pole placement. Considering the system in its state space form as:

$$\begin{aligned}\dot{x} &= Ax + Bu \\ y &= Cx + Du\end{aligned}\tag{2.9}$$

The necessary and sufficient condition to apply the pole placement control is the reachability of the pair (A, B) , that was always verified.

The control law is:

$$u(t) = -Kx(t)\tag{2.10}$$

so that the closed-loop state equation is:

$$\dot{x} = (A - BK)x(t)\tag{2.11}$$

The aim of pole placement control is to create a matrix K so that the eigenvalues of $(A - BK)$ are arbitrarily assigned to stabilize the system and to improve the performance of the controlled system.

The poles were tuned to ensure stability and the best performance of the system, obtaining:

$$P = [-34 + i, -34 - i, -36, -37, -38, -39, -40]\tag{2.12}$$

Notice that the selected poles should also avoid the actuators to saturate, so they cannot be too large in absolute value.

In order to determine the gain K , MATLAB command `place` was used.

The poles were initially selected leaving only one pole much smaller than the others, so that it could be approximated to a first-order system (or two complex and conjugate poles with much smaller real part, to have a second-order system). But this approximation did not work properly, probably because of the high number of states of the system. Then, the poles were chosen to be near one to each other.

To avoid steady-state error, an integrator must be added to the control system. To include it, the state is extended and the new matrices are used as inputs of the function `place`, to place 7 poles (instead of 6), getting the matrix K with 7 gains.

An important parameter is α , which was used to force all the poles to have absolute value larger than that. This allows to increase the robustness of the system and to improve its performance, moving the poles further from the imaginary axis.

Pole placement was only used for position control, because it is a simple technique, but it is not much practical to tune, in particular with high-order systems such as this one.

Finally, pole placement is a full state-feedback control strategy, for which all the state variables must be known. Nonetheless, not all of them are measured, so a state observer is needed. The variables that are assumed to be measurable are θ_2 and θ_3 , while the motor measurement is not used, because the potentiometer is too noisy and leads to stability issues. The observer is designed defining the gain L by pole placement. The procedure is the same as the one explained above, using the same MATLAB function.

The selected poles are:

$$P_o = [-12, -80, -100, -120, -130, -140] \quad (2.13)$$

These poles can be larger than the ones selected for the regulation, because there are not actuators that risk to saturate.

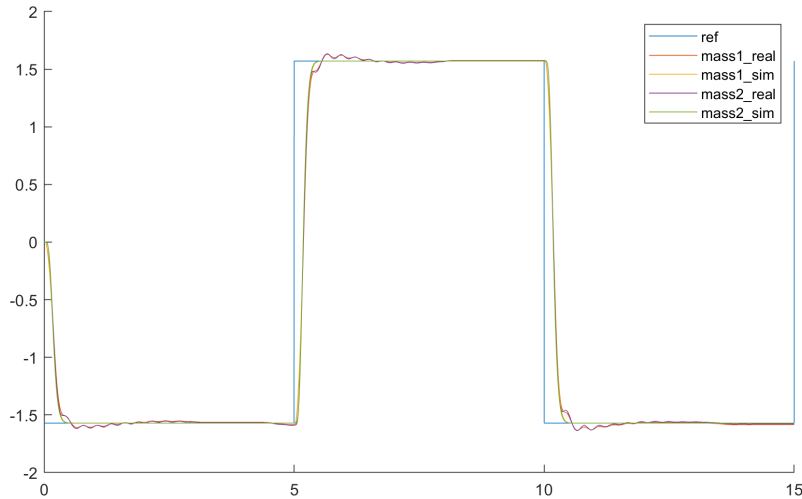


Figure 2.11: Pole placement for position: reference tracking

	Rise Time	Settling time 3%
Real system	0.182 s	0.474 s
Simulated system	0.174 s	0.342 s

The figure shows the result of the designed control for the tracking of a reference. As reported in the table, the settling time is short (< 0.5 s) and the overshoot is low.

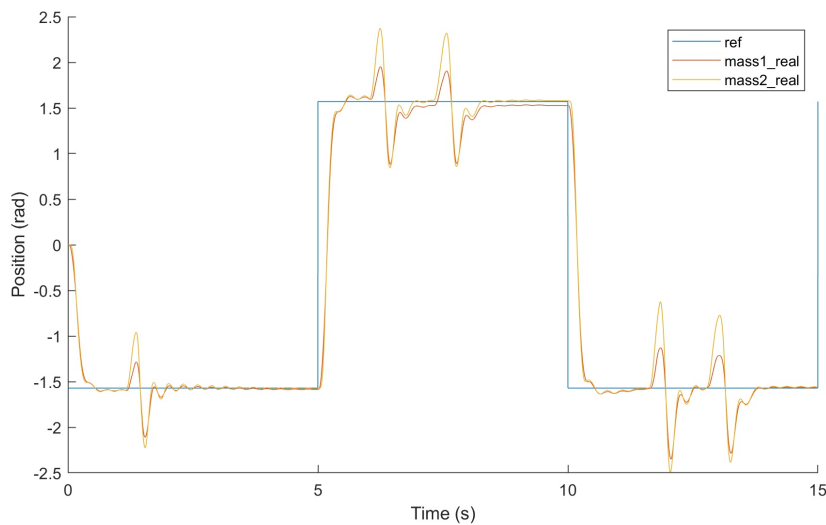


Figure 2.12: Pole placement for position: disturbance rejection

The second figure shows the effect of the designed control on external disturbances. The peaks are disturbances physically applied on the mass, their effect is reduced very quickly by the control action.

The action of the control law is clear if the input voltage is plotted. In the plot, voltage peaks appear in correspondence of the disturbances.

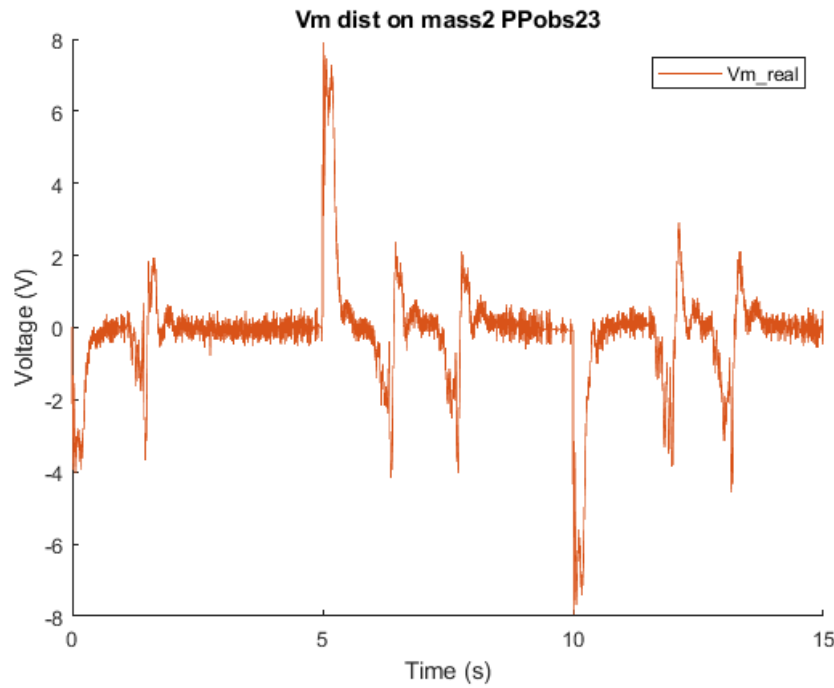


Figure 2.13: Pole placement control, input voltage of disturbed system

LQinf control Linear Quadratic control theory (LQ) was applied for regulation. This technique allows to find the optimal gain K to minimize a function that includes both the states and the input of the system, weighted respectively by matrices Q and R .

The MATLAB function `lqr` was used, so that the problem was automatically solved and K was found, given the matrices of the state-space system and of the weights.

Even LQ is a full state-feedback control strategy, so an observer must be designed to estimate all the state variables. In particular, two cases are considered: either both the load angles measurements are available, or only the measurement of the first load angle is. In the first case, the observer is the same used for pole placement. In the latter case, the poles of the observer were moved to guarantee a better estimation with the only available measurement.

For this latter observer, the poles were

$$P_o = [-20, -40, -45, -50, -55, -60] \quad (2.14)$$

As before, an integral action is included in the control system, so that the steady-state error tends to zero. To include it, the state is extended and the `lqr` function is applied to the matrices of the extended state.

Finally, as before, an additional parameter α was tuned, moving the poles of the system by its value. This is important to guarantee robustness (poles are further from the imaginary axis), but also for the performance of the control action. Weight matrices Q and R were tuned starting from the standard ones:

$$Q = CC^T \quad R = I_m \quad (2.15)$$

Since the input voltage was noisy, in some cases the matrix R was increased to make the noise smaller than the sensitivity of the motor. In this way, the input noise had not any effect on the motor.

LQR was used both for position and speed control, since it resulted easier to tune and more effective than pole placement.

2.4.1 Position Control

Reference Tracking Both measurements are available.

Gain matrix:

$$K = [203.9, 2.3, -153.9, 3.0, 76.8, 2.4, -777.7] \quad (2.16)$$

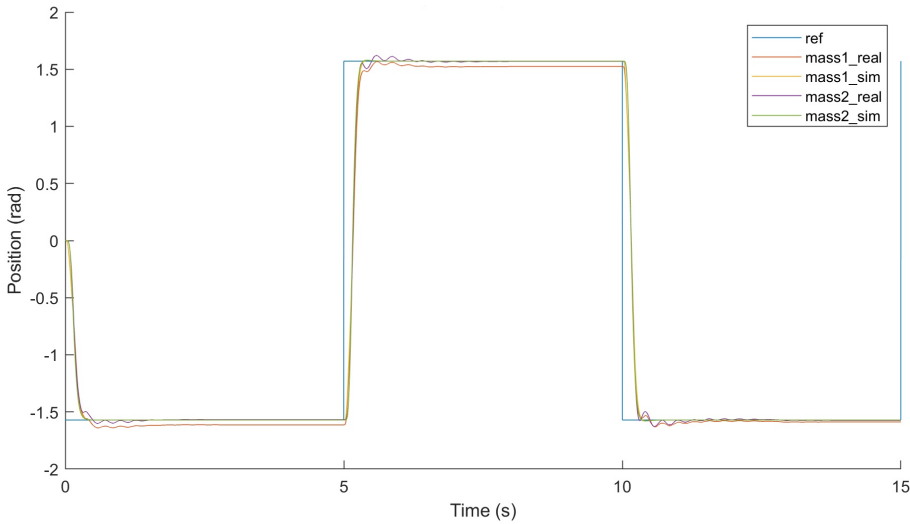


Figure 2.14: LQR, measuring both θ_2 and θ_3

	Rise Time	Settling time 3%
Real system	0.162 s	0.424 s
Simulated system	0.144 s	0.292 s

Only θ_2 measurement is available.

Gain matrix:

$$K = [203.7, 2.3, -154.0, 3.0, 75.8, 1.8, -774.8] \quad (2.17)$$

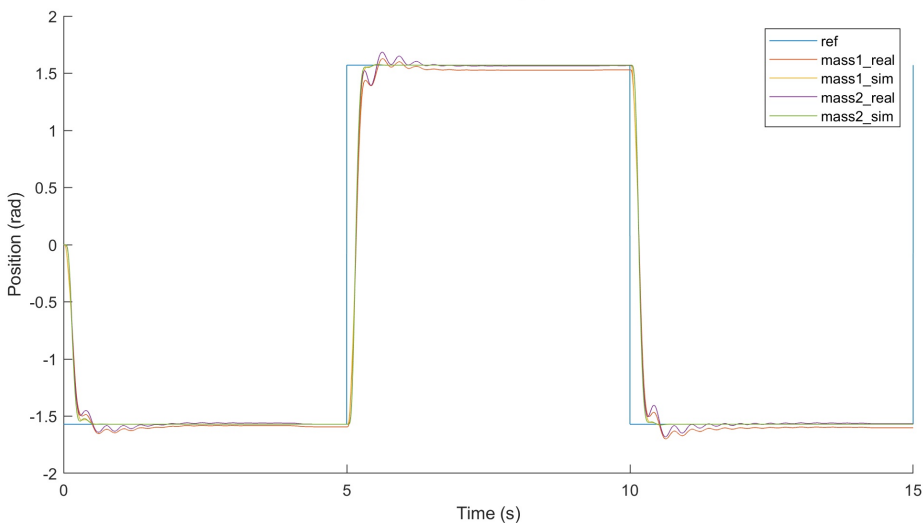


Figure 2.15: LQR, measuring only θ_2

	Rise Time	Settling time 3%
Real system	0.148 s	0.958 s
Simulated system	0.128 s	0.390 s

Since LQ looks for an optimal solution, it should return the best gain matrix K if it is properly tuned. The result is a closed-loop system that has the best characteristics, referring to the settling and rise time. The figures show that the tracking is very fast, in both the cases. In the first case, the settling time is less than 0.5 s; in the second case it is less than 1 s. The latter one is still a good result, considering that only the control of the second mass was performed only measuring the angle of the other one.

LQG LQG combines the LQ control for the closed-loop regulator with the Kalman Filter used as an observer. Noises on the measurements of this system were assumed to be negligible, because only the encoders were used as inputs of the observer. The errors of the encoders are due only to their step, that have small values with respect to the angles in this report and thus can be neglected.

Then, the duality LQR-KF was exploited and the Kalman Filter was applied to the observer in a way that is similar to the LQR. So, the function `lqr` was applied to define the gain matrix of the observer K_o , changing the function inputs to satisfy the duality.

Even for LQG, the two cases are considered, when both measurements are available and when only the one of the first mass is.

If both measurements are available, the gain matrix of the controller is:

$$K = [203.9, 2.3, -153.9, 3.0, 76.8, 2.4, -777.7] \quad (2.18)$$

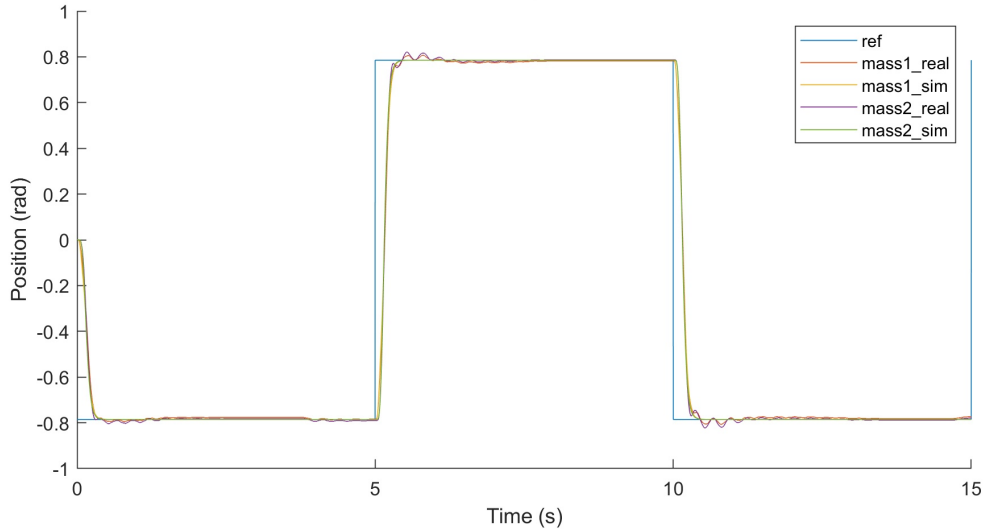


Figure 2.16: LQG, measuring both θ_2 and θ_3

	Rise Time	Settling time 3%
Real system	0.142 s	0.270 s
Simulated system	0.144 s	0.292 s

If only θ_2 is available, the gain matrix is:

$$K = [203.7, 2.3, -154.0, 3.0, 75.8, 1.8, -774.8] \quad (2.19)$$

	Rise Time	Settling time 3%
Real system	0.146 s	0.904 s
Simulated system	0.128 s	0.390 s

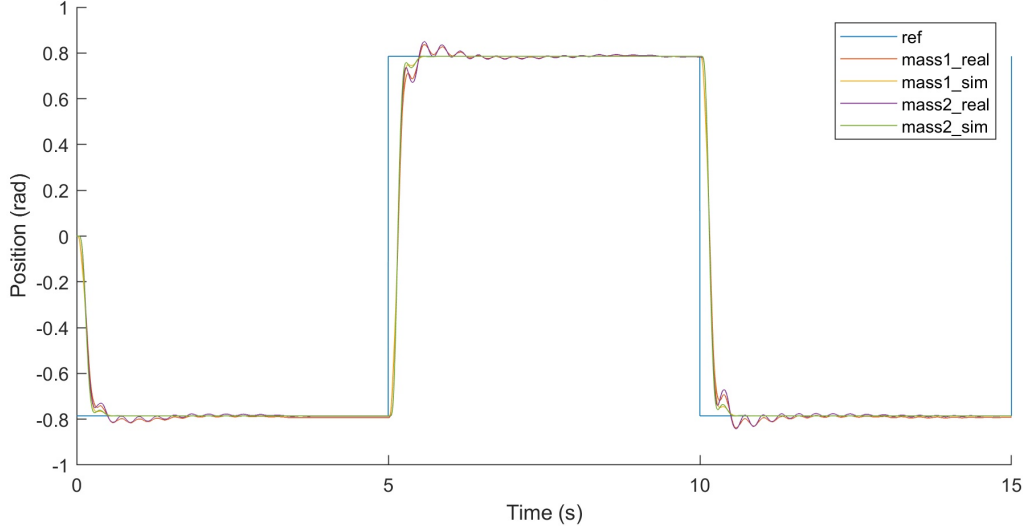


Figure 2.17: LQG, measuring only θ_2

The figures and the tables show how the designed control allows to get good performances. Particularly in the first case, the settling time is very short (< 0.3 s) and the measured output for both the masses is always very close to the reference. This is a natural consequence of the applied strategy: LQG looks for the optimal solution for both the regulator and the observer, guaranteeing better performance in the state estimation and in the definition of the gain matrix.

Disturbance on Mass 2 LQR and LQG defined above are used to control the system when it is subject to external disturbance. In particular, a physical disturbance was applied to the mass 2, moving it from the position that it should hold. The performance regarding the reduction of disturbances is evaluated for both the control strategies.

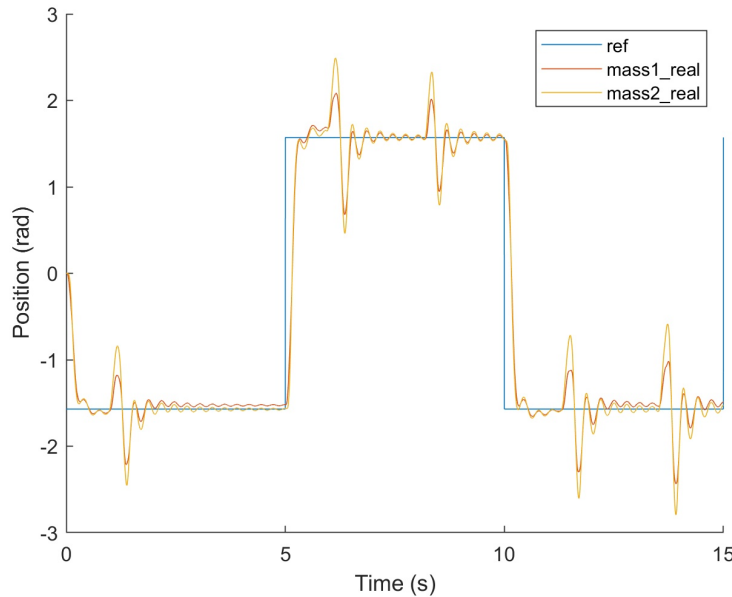


Figure 2.18: LQR, external disturbance

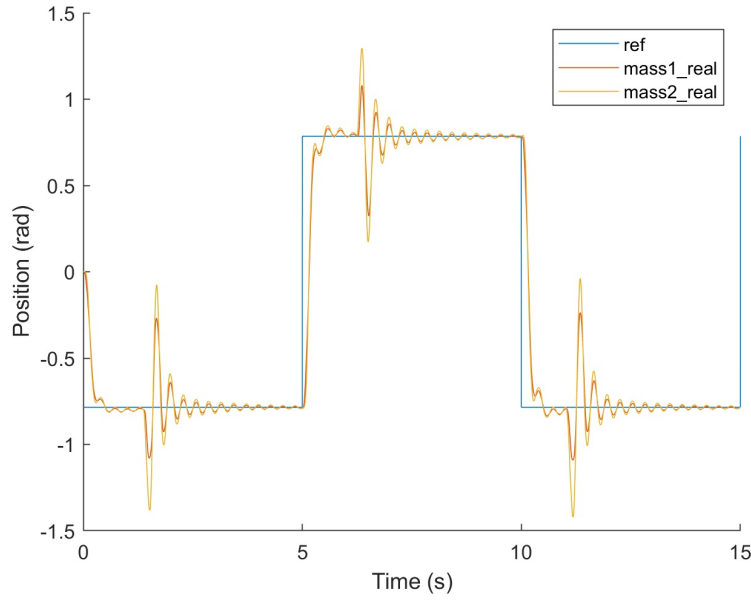


Figure 2.19: LQG, external disturbance

In the figures, the response of the system to disturbances are shown. For both LQR and LQG, the effect of the disturbances is reduced very quickly and the position is recovered even though the disturbance is large.

The figure below shows the input voltage when disturbances are applied to the system controlled by LQG. The voltage peaks correspond to the reaction of the controller to the external disturbances.

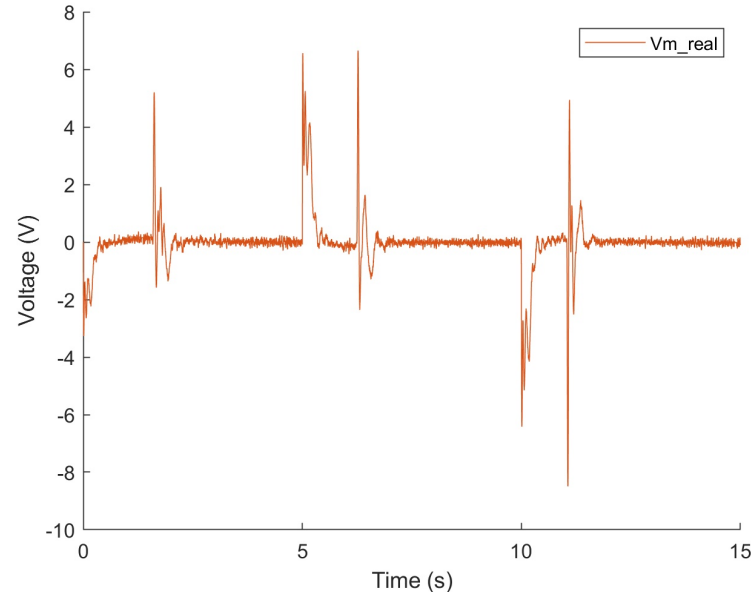


Figure 2.20: LQG, input voltage

2.4.2 Speed Control

Reference Tracking For the speed control, three solutions were defined.

If both measurements are available, two control strategies were developed, depending on the observer design: one of them used Pole Placement, the other one used Kalman Filter, similarly to the position control. If only the measurement of the first mass was available, the observer was designed directly with the Kalman Filter, since it was proven to be the most practical and effective one.

If both measurements are available, the gain matrix with LQR is:

$$K = [309.6, 2.9, -81.4, 7.5, 94.2, 6.9, -2313.3] \quad (2.20)$$

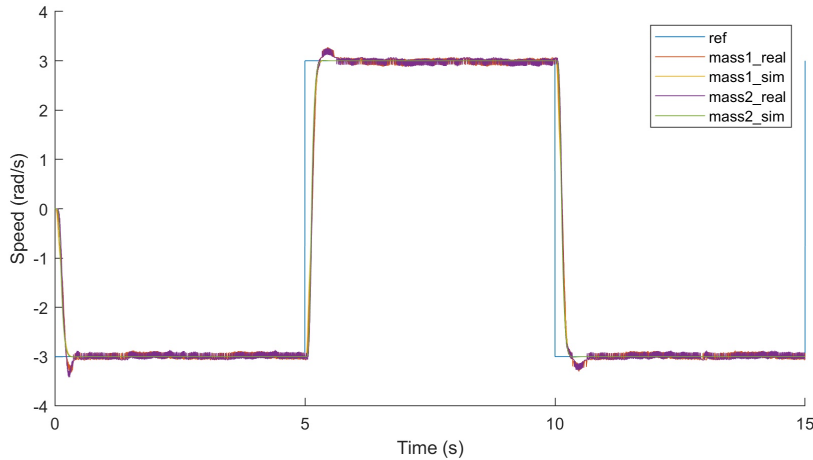


Figure 2.21: LQR, with both the measurements available

	Rise Time	Settling time 3%
Real system	0.104 s	0.474 s
Simulated system	0.120 s	0.246 s

Whereas the gain matrix with LQG is:

$$K = [309.6, 2.9, -81.4, 7.5, 94.2, 6.9, -2313.3] \quad (2.21)$$

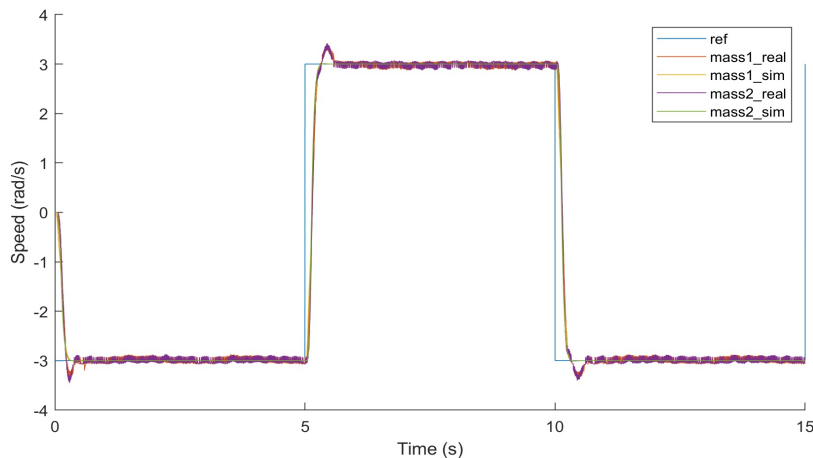


Figure 2.22: LQG, with both the measurements available

	Rise Time	Settling time 3%
Real system	0.104 s	0.486 s
Simulated system	0.120 s	0.246 s

If only the measurement of θ_2 is available, the gain matrix with LQG is:

$$K = [309.6, 2.9, -81.4, 7.5, 91.3, 5.2, -2313.3] \quad (2.22)$$

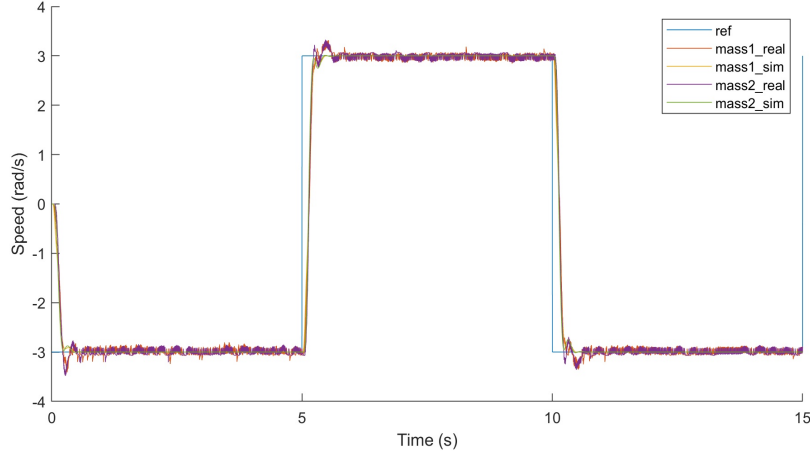


Figure 2.23: LQG, with only θ_1 available

	Rise Time	Settling time 3%
Real system	0.104 s	0.744 s
Simulated system	0.120 s	0.358 s

All the proposed solutions allow the second mass to reach the reference in a short time. In particular, as it was expected, the LQG control gives the best performance. However, it is important to notice that also the control of the second mass without measuring its angle has a very good settling time.

Disturbance on Mass 2 The same LQG control was used also to test the capability of the controlled system to reduce the external disturbances.

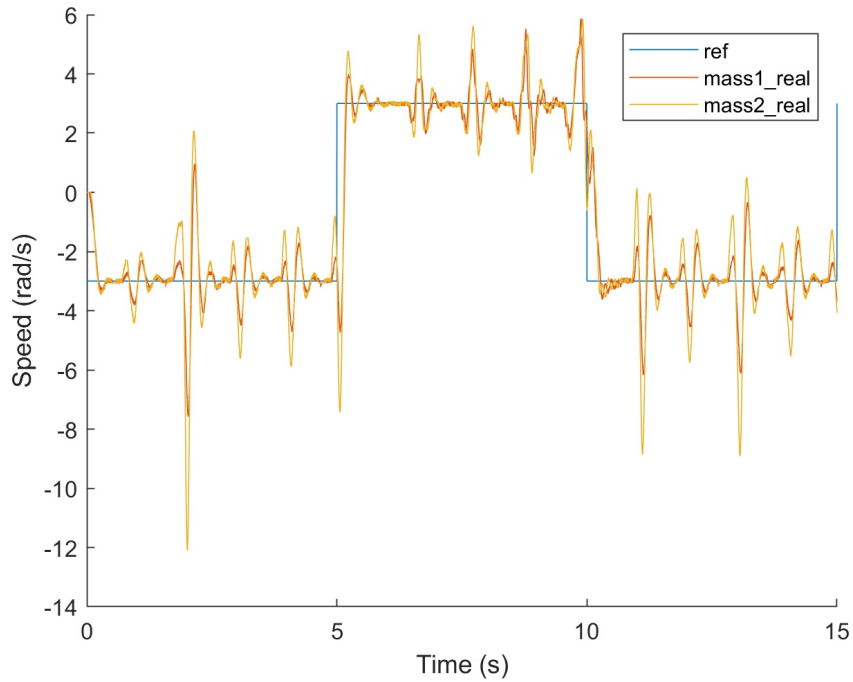


Figure 2.24: LQG, system subject to disturbances

In the figure, all the peaks are physical disturbances applied directly to the second mass. The response of the system is very fast: though many disturbances are applied, the response is so fast that the speed reference is always recovered before the following disturbance is applied.

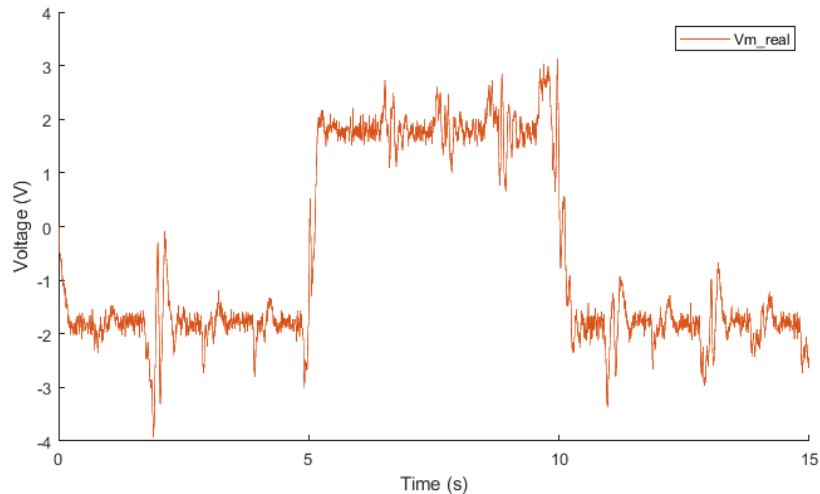


Figure 2.25: Input voltage to system subject to disturbances

3 Conclusions

The system presented a main problem that was not easy to deal with: the low damping due to the spring. This criticality affected the approach, since it made the system hard to control, highly oscillating and easily subject to instability.

In particular, the first part of the work is characterized by the effort to reduce the effect of the low damping by directly acting on it. Once the PID resulted not suitable to control this system, noticing that the performance was always affected mainly by issues related to the resonance, the idea was to try and counter it. The developed solution deals perfectly with the peak and represents probably the most aggressive way to face it. With this control strategy, the results are excellent, both for position and speed control. The system is high performance, fast and with small overshoot.

In the second part of the work, the control problem was solved much more easily. The MIMO control strategies allow to act directly on the poles, bypassing the issue related to the low damping. It is enough to choose properly the poles in pole placement approach, or to tune the weight matrices of the LQ, to get a system that has good performance. The controlled system never presents residual oscillations once the reference is reached (unlike the one mass system), so the two resonance frequencies are never shown clearly. LQG control gave the best results, allowing to get a very fast system. Also the other techniques were designed properly and gave excellent results.

For both the systems, reference tracking was always performed in less than one second. In many cases, in less than 0.5 s. The best result is obtained by LQG control for position, with which the reference is reached in 0.27 s, that is a great result.

Also the disturbance attenuation is performed very well by both the controlled systems. The input voltages show that the control action always reacts to the external disturbances, trying to take the mass back to the position/speed reference that it had to hold.

Finally, the control of the second mass was performed with good results also when only the measurements of the first mass were available. This was possible thanks to a well-designed state observer, which allowed to estimate accurately the missing measurement. Once the state was estimated properly, it was easier to get good results with the control action.

$$P_{obs23} = [-28, -37 + 25i, -37 - 25i, -39 + 65i, -39 - 65i, -40] \quad (3.1)$$

$$K = [204, 2.3, -154, 3, 76, 1.8, -775] \quad (3.2)$$

$$L_{obs23} = \begin{bmatrix} 54 & 29 \\ -318 & -180 \\ 101 & 15 \\ 3232 & 1261 \\ 15 & 82 \\ 927 & 1858 \end{bmatrix}$$

(3.3)

$$J_1\ddot{\theta}_1 + B_1\dot{\theta}_1 + k_s(\theta_1 - \theta_2) = \tau_1 \quad (3.4)$$

$$J_2\ddot{\theta}_2 + B_2\dot{\theta}_2 + k_s(\theta_2 - \theta_1) + k_s(\theta_2 - \theta_3) = 0 \quad (3.5)$$

$$J_3\ddot{\theta}_3 + B_3\dot{\theta}_3 + k_s(\theta_3 - \theta_2) = 0 \quad (3.6)$$